Applied Catalysis B: Environmental 142–143 (2013) 241–248

Contents lists available at SciVerse ScienceDirect

Applied Catalysis B: Environmental

journal homepage: www.elsevier.com/locate/apcatb

Catalytic valorization of CO_2 *via* methanol synthesis with Ga-promoted Cu–ZnO–ZrO_2 catalysts

Rosa Ladera [a], Francisco J. Pérez-Alonso [a], Juan M. González-Carballo [b,1], Manuel Ojeda [c,1], Sergio Rojas [a,*], José Luis G. Fierro [a,**]

[a] Group of Sustainable Energy and Chemistry, Institute of Catalysis and Petrochemistry (CSIC), C/Marie Curie 2, 28049 Madrid, Spain
[b] Sasol Technology (UK) Ltd, Purdie Building, North Haugh, St Andrews, Fife KY16 9ST, United Kingdom
[c] BP Chemicals Ltd, Saltend, Hull HU12 8DS, United Kingdom

ARTICLE INFO

Article history:
Received 31 January 2013
Received in revised form 9 May 2013
Accepted 12 May 2013
Available online 18 May 2013

Keywords:
CO_2
Hydrogenation
Methanol
Ga
Promoter

ABSTRACT

New technologies aimed to reduce the huge amounts of anthropogenic CO_2 emissions and their environmental impacts would only succeed if the product resulting from the transformation of CO_2 is demanded in high quantities, as for instance, methanol. In this context, we have undertaken a systematic study of the catalytic hydrogenation of CO_2 into methanol with Ga-doped Cu/ZnO/ZrO_2 catalysts. The detailed characterization of these systems reveals that the abundance of surface Cu and the amount of metallic Cu^0 increases with Ga_2O_3 loading. These features are responsible for a selectivity enhancement in CH_3OH synthesis from CO_2/H_2 mixtures. Furthermore, the reaction kinetic analysis shows that the production of CH_3OH is increased at high temperatures by increasing H_2 pressure. These results are very important for the development and implementation of highly active industrial catalysts for the synthesis of methanol from CO_2 and H_2

1. Introduction

Dwindling fossil fuels and impending climate change are major energy, environmental and economic issues all over the world. Climate changes that are largely driven by the greenhouse gas emissions from fossil fuels threaten human lives and the Earth's biosphere [1]. Accordingly, CO_2 recycling is nowadays under increased scrutiny as one of the possible contributions to CO_2 mitigation and as an opportunity to use a low-cost carbon source. Any technology aimed to reduce its environmental impact would only succeed if the product obtained from the transformation of CO_2 is demanded in high quantities. This implies that CO_2 should be transformed either to fuels or to highly demanded commodities.

A possible route is the synthesis of hydrocarbons from CO_2 hydrogenation. This process is akin to the Fischer Tropsch synthesis (FTS), but using CO_2 instead of CO in the feed gas [2–4]. This feature limits the catalysts for this process to Fe-based ones, since they are active in both water–gas shift ($CO + H_2O \rightarrow CO_2 + H_2$, WGS) and FTS reactions.

Another interesting option is the transformation of CO_2 into oxygenated chemicals, such as methanol. The importance of methanol in today's industry cannot be neglected. Methanol is amongst the top ten commodity chemicals; its production accounts to more than 30 MMT/year. The main uses of methanol are as a fuel, either pure (see direct methanol fuel cells) or blended. Furthermore, it is the raw material to producing olefins (methanol-to-olefins, MTO) and gasoline (methanol-to-gasoline, MTG). Methanol is also a key intermediate for the production of chemicals such as formaldehyde, dimethyl ether (DME), methyl *tert*-butyl ether (MTBE) and acetic acid to name but a few [5]. The synthesis of CH_3OH from syngas is a high temperature and high-pressure, exothermic, equilibrium-limited reaction. ZnO/Cr_2O_3 catalysts were used in the early stages of the process until ICI developed the archetypal Cu/ZnO/Al_2O_3 based catalyst, which operates at 493–548 K and 5–10 MPa. Due to equilibrium constrains, maximum conversion is maintained well below 25% to avoid the formation of undesired products such as DME, CH_4 and especially, CO_2 when is used syngas and CO when the synthesis is from CO_2 and H_2. The formation of CO accounts to the reverse water–gas shift reaction (RWGS, $CO_2 + H_2 \rightarrow CO + H_2O$) for which Cu is among the most active catalysts [6]. In fact, RWGS is considered as the main side reaction of the CH_3OH synthesis from CO_2 and H_2 [7].

Although methanol is currently produced from CO/H_2 mixtures, the presence of CO_2 in the reactants feeding increases considerably the observed reaction rates [8]. However, at high concentrations,

* Corresponding author. Tel.: +34 915854632; fax: +34 653 858 987.
** Corresponding author. Tel.: +34 915854769.
E-mail addresses: srojas@icp.csic.es (S. Rojas), jlgfierro@icp.csic.es (J.L.G. Fierro).
[1] Current address.

0926-3373/$ – see front matter © 2013 Elsevier B.V. All rights reserved.
http://dx.doi.org/10.1016/j.apcatb.2013.05.019

CO_2 may inhibit CH_3OH synthesis [9]. The actual nature of the active site of Cu/ZnO-based catalysts is a topic of debate and different groups suggest the predominant role of Cu^0, Cu^0/Cu^+ ensembles or Cu/ZnO or Cu/Zn alloys/interphases. Furthermore, some authors have reported that the nature of the catalyst evolves during the reaction, yielding to the identification of Cu particles on ZnO and/or ZnO on Cu particles [10]. These researchers found and identified the formation of Cu–Zn α-brass alloy upon reduction treatment at 673 K by *in situ* X-ray absorption spectroscopy (XAS) studies as the active sites for methanol synthesis with SiO_2-supported Cu/ZnO catalysts. Irrespectively of the actual nature of the active site, Cu dispersion is a crucial parameter that determines the catalyst activity for the production of methanol; therefore, it is highly desirable to synthesize catalysts showing high Cu dispersion. For this end, a variety of promotional elements have been studied [11–13]. More specifically, Saito et al. explored the influence of Ga_2O_3 as structural promoter in multimetallic CuZnZrAl on Pd-based catalysts for the synthesis of methanol [14–17]. Inui et al. demonstrated more than a decade ago that the addition of Ga_2O_3 to Cu–ZnO–Cr_2O_3–Al_2O_3 catalysts resulted in an enhanced catalytic activity for CO_2 hydrogenation to methanol [18]. More recently, Toyir et al. have also reported a positive effect of Ga addition to SiO_2-supported Cu catalysts on methanol synthesis rates *via* CO_2 hydrogenation [19,20].

Here, we report a detailed and systematic study of the effects of Ga addition on Cu/ZnO/ZrO_2 catalysts for the synthesis of methanol from CO_2/H_2 reactants. Catalysts characterization data reveal that the overall concentration of copper species, as well as metallic Cu^0, on the surface increases with the amount of Ga_2O_3 in the catalysts. Combined, these features result in more active and more selective catalysts for the synthesis of methanol from CO_2/H_2 mixtures. Furthermore, a detailed kinetic analysis of the reaction points out that at high reaction temperatures, methanol productivity is increased upon increasing the H_2 pressure. These results are very important for the development and implementation of highly active industrial catalysts for the synthesis of methanol from CO_2.

2. Experimental

2.1. Catalysts preparation

A series of solids containing a fixed concentration of CuO and ZnO (50 and 15 wt.%, respectively) and different amounts of ZrO_2 and Ga_2O_3 were prepared by co-precipitation of the different metal precursors at controlled pH. Firstly, a precipitate was formed by simultaneous adding an aqueous solution of Na_2CO_3 (1.1 M) and an aqueous solution containing the metal precursors, *i.e.*, $Cu(NO_3)_2{\cdot}2.5H_2O$ (ACS reagent, 98%), $Zn(NO_3)_2{\cdot}6H_2O$ (98%), $ZrO(NO_3)_2{\cdot}xH_2O$ (>99%) and $Ga(NO_3)_3{\cdot}xH_2O$ (99.999%) to hot water. The mixture was kept under stirring at 343 K and constant pH (∼7) during the co-precipitation, and further aged for 12 h at room temperature. The obtained solid was washed with deionized hot H_2O and then recovered by filtration. This process was repeated several times until the pH of the filtrate was 7.0 ± 0.2. The solid was subsequently dried in ambient air at 343 K and then treated (calcined) at 673 K in ambient air for 4 h (based on thermogravimetric analyses). The obtained solids were hereafter referred to as CZZ for those containing CuO, ZnO and ZrO_2, and Ga_x-CZZ for the Ga-modified CZZ, where *x* denotes the weight percentage of Ga_2O_3 in the solid. Table 1 summarizes the nomenclature and chemical composition (oxide base) of all prepared samples.

2.2. Characterization techniques

Thermogravimetric analyses (TGA) were performed on a Mettler Toledo microbalance TGA/SDTA 851. The sample (*ca.* 20 mg) was placed in a crucible and the temperature was increased from 323 to 1100 K at 10 K min^{-1} while flowing a 20 vol.% O_2/N_2 mixture (250 cm^3 min^{-1}).

X-ray diffraction patterns were recorded using Cu Kα radiation in a Seiffert 3000 XPert X-ray diffractometer. Diffractograms were registered within the 2θ = 15–80° diffraction angles, and phase identification was carried out by comparison with patterns from the International Centre for Diffraction Data (ICDD) database.

Brunauer–Emmett–Teller (BET) specific surface areas, pore volume, and pore size distribution of the samples were obtained from N_2 adsorption–desorption isotherms measured at 77 K with a Micromeritics ASAP 2000 apparatus. The samples were degassed at 413 K for 16 h prior to the physisorption measurements.

Temperature-programmed reduction (TPR) experiments were carried out with a Micromeritics TPR/TPD 2900 instrument in a quartz U-tube microreactor. Prior to the reduction, the sample (*ca.* 50 mg) was pretreated in flowing He at 393 K for 1 h and then cooled down to room temperature. Afterwards, a 10 vol.% H_2/Ar flow (50 cm^3 min^{-1}) was passed over the sample while heating at a rate of 10 K min^{-1} from room temperature to 1173 K.

X-ray photoelectron spectra (XPS) were acquired with a VG Escalab 200 R spectrometer in the pulse-count mode at a pass energy of 50 eV using a Mg Kα ($h\nu$ = 1253.6 eV) X-ray source. Kinetic energies of photoelectrons were measured using a hemispherical electron analyzer working at a constant (20 eV) pass energy. The powder samples were pressed into stainless steel holders and then mounted on a support rod placed in the pretreatment chamber. The XPS data were signal averaged for at least 200 scans and were taken in increments of 0.1 eV with dwell times of 50 ms. Binding energies were calibrated relative to the C 1s peak at 284.6 eV to correct the contact potential differences between the sample and the spectrometer. Peak quantification was done by subtracting Shirley type backgrounds. For the *in situ* analysis, the samples were thermally treated in H_2 at 573 K for 2 h in the pre-treatment chamber and then transferred to the analysis chamber without contact with ambient air.

Table 1
Nomenclature, chemical composition, and characterization data (surface area, CuO and Cu crystallites size, and exposed Cu^0 area) of unpromoted and Ga-promoted CZZ solids.

Sample	Composition (wt.%)				Area (m^2 g^{-1})[a]	Size (nm)[b]		Cu^0 (m^2 g^{-1})[c]
	CuO	ZnO	ZrO_2	Ga_2O_3		CuO	Cu	
CZZ	50	15	35.0	0.0	129	6	8	11.3
$Ga_{0.2}$-CZZ	50	15	34.8	0.2	124	4	8	11.9
$Ga_{0.5}$-CZZ	50	15	34.5	0.5	127	4	7	13.1
$Ga_{1.0}$-CZZ	50	15	34.0	1.0	109	–	9	12.8
$Ga_{3.0}$-CZZ	50	15	32.0	3.0	102	–	7	13.5

[a] BET surface area determined from N_2 adsorption–desorption experiments.
[b] Mean crystallites size calculated from XRD.
[c] Exposed metallic Cu^0 determined from N_2O chemisorption measurements.

The amount of exposed metallic Cu^0 (S_{Cu}) was evaluated by dissociative N_2O chemisorption method (see Eq. (1)) described by Chinchen et al. [21,22]:

$$2Cu_{(s)} + N_2O_{(g)} \rightarrow Cu_2O_{(s)} + N_{2(g)} \quad (1)$$

where $Cu_{(s)}$ denotes a surface copper atom. A catalyst sample (*ca.* 50 mg) was placed in a quartz tube reactor and reduced at 573 K in an H_2/N_2 mixture (10 vol.%, 100 cm^3 min^{-1}). Temperature-programmed reduction (TPR) experiments confirmed that this reduction procedure (heating rate of 10 K min^{-1}, 573 K, 1 h) is sufficient to reduce the CuO to the metallic Cu species. After reduction, the catalyst was cooled down to 333 K (chemisorption temperature) under flowing N_2. Then, a $N_2O/Ar/N_2$ mixture (0.1 vol.% N_2O, 0.1 vol.% Ar, 50 cm^3 min^{-1}) was introduced in the reactor until the reaction was completed. N_2O consumption was monitored with a mass spectrometer (Baltzer Prisma QMS 200). The copper surface area was calculated assuming an atomic copper surface density of 1.46×10^{19} at. Cu m^{-2} and a molar N_2O/Cu stoichiometry equals to 0.5 [21,22].

2.3. Catalytic activity measurements

Methanol formation *via* CO_2 hydrogenation was evaluated in a fixed-bed continuous flow reactor. The catalyst (0.2 g, 0.25–0.30 mm pellet size) was mixed with SiC (2.0 g, 0.25–0.30 mm pellet size) and the mixture was introduced in the reactor between wool plugs. The catalyst was pretreated with a 10 vol.% H_2/N_2 flow at 573 K for 1 h. Thereafter, the temperature was decreased to 463 K in N_2 and the catalyst was subsequently exposed to the reactants H_2/CO_2 (3:1 molar ratio, 15,000 cm^3 $h^{-1}g_{cat}^{-1}$) at 3.0–7.0 MPa. Catalytic activity was measured at 463, 483, 503, 523 and 573 K. The gas products were analyzed on line with a gas chromatograph (Varian CP-3800) equipped with thermal conductivity and flame ionization detectors. CO_2 conversion and products selectivity were calculated as follows:

$$CO_2 \text{ conversion} : X_{CO_2} = \frac{(F_{CO_2})_{in} - (F_{CO_2})_{out}}{(F_{CO_2})_{in}} \quad (2)$$

where $(F_{CO_2})_{in}$ and $(F_{CO_2})_{out}$ are the inlet and outlet CO_2 molar flowrates, respectively

$$\text{Product } i \text{ selectivity} : S_i = \frac{(F_i)_{out}}{(F_{CO_2})_{in} - (F_{CO_2})_{out}} \quad (3)$$

where $(F_i)_{out}$ is outlet molar flowrate of product *i*. CH_3OH formation rates are reported as the number of molecules formed per unit time and per catalyst weight (mmol h^{-1} g_{cat}^{-1}).

3. Results and discussion

3.1. Catalysts characterization

Based on the corresponding thermogravimetric analyses, which show a moderate weight loss between 298 and 650 K (data not shown), all samples were treated in ambient air at 673 K for 4 h. The specific surface area (BET) of these calcined solids is depicted in Table 1. Substitution of ZrO_2 by Ga_2O_3 does not affect significantly measured surface areas in those samples with low Ga_2O_3 contents (<0.5 wt.% Ga_2O_3), but results in a moderate decreasing of the area values (*ca.* 20%) when the solids contain higher Ga_2O_3 loadings.

Fig. 1 (left panel) shows the X-ray diffraction profiles of the samples calcined in ambient air at 673 K for 4 h. The set of reflections at 2θ values of 35.5, 35.6 and 38.7° and at 2θ values of 31.8, 34.5 and 36.3° accounts to the presence of crystalline domains of CuO and ZnO, respectively. The presence of ZrO_2 results in the continuous raising of the background intensity within the 2θ range where the most intense lines for the monoclinic and tetragonal ZrO_2 phases (2θ–30°) are present [23]. Noticeably, the intensity of the reflections ascribed to CuO phase decreases with the increasing Ga_2O_3 content, even disappearing in the diffractograms of samples $Ga_{1.0}$-CZZ and $Ga_{3.0}$-CZZ. The average crystallite sizes of the CuO

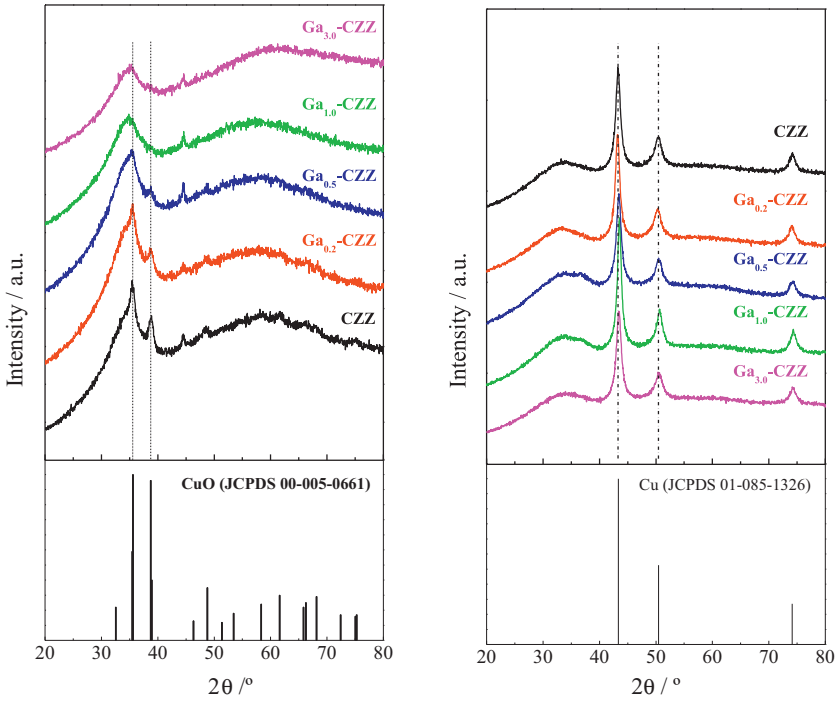

Fig. 1. X-ray diffractograms of the samples calcined under ambient air at, 673 K, 4 h (left panel) and of the reduced samples under H_2 at 573 K, 1 h (right panel). X-ray diffraction patterns of CuO and Cu phases are shown for reference.

Table 2
Surface atomic ratios derived from XPS analyses of the calcined (ambient air, 673 K, 4 h) and reduced (H_2, 573 K, 1 h) samples.

Sample	Calcined			Reduced		
	Zn/Cu	Zr/Cu	Ga/Cu	Zn/Cu	Zr/Cu	Ga/Cu
CZZ	0.56	0.85	–	0.77	1.22	–
$Ga_{0.2}$-CZZ	0.54	0.82	–	0.74	1.01	–
$Ga_{0.5}$-CZZ	0.52	0.79	0.01	0.64	0.79	0.01
$Ga_{1.0}$-CZZ	0.43	0.72	0.02	0.56	0.67	0.01
$Ga_{3.0}$-CZZ	0.44	0.65	0.06	0.57	0.75	0.09

domains (reported in Table 1) were determined from the Scherrer equation. In line with the above observation, the average CuO size decreases with the increasing content of Ga_2O_3 in the samples. The size of CuO crystallites in the CZZ sample is *ca.* 6 nm, and slightly decreases to *ca.* 4 nm in the samples with low Ga contents (0.2 and 0.5 wt.% Ga_2O_3). For the samples with higher Ga contents (1 and 3 wt.% Ga_2O_3), no diffraction peaks ascribed to Cu-containing phases are detected. This observation suggests that the dispersion of the CuO domains increases for the Ga-containing catalysts due to the character of structural promoter of Ga_2O_3, which increases the resistance of CuO to sinter during the thermal treatment [23].

The reducibility of the calcined samples was investigated by temperature programmed reduction (TPR) experiments (not shown). All samples exhibit a single H_2 consumption peak ascribed to the reduction of CuO to metallic Cu. The reduction peak is centred at 468 K in the case of the unpromoted CZZ sample, but is shifted to higher temperatures (~486 K) for all Ga-containing samples. Based on these data, all samples were pretreated in H_2 at 573 K for 1 h before measuring the catalytic activity in CO_2/H_2 reactions.

Fig. 1 (right panel) shows the X-ray diffractograms of the reduced samples. The main diffraction peaks observed at 2θ equals to 43.3, 50.5 and 74.1° are ascribed to metallic Cu. Peaks ascribed to CuO are now not observed in the diffractograms. The size of the Cu^0 domains on the reduced samples, as determined from the Scherrer equation (Table 1), is very similar in all samples (7–9 nm). Clearly, the thermal treatment in H_2 at 573 K is sufficient to produce bulk Cu^0 crystallites from CuO. Nonetheless, the presence of partially oxidized copper species, typically Cu^+, cannot be ruled out completely.

Table 2 summarizes the relative abundance of the different elements as recorded by X-ray photoelectron spectroscopy. The Cu $2p_{3/2}$ core level region of the calcined samples (Fig. 2A) show a single peak centred at binding energies between 934.1 and 934.5 eV. This binding energy and the presence of intense satellite lines at *ca.* 8.3 eV above the principal Cu $2p_{3/2}$ line indicate unambiguously the presence of Cu^{2+} species, more likely as CuO [19]. The Zn $2p_{3/2}$ core level region appears as a single peak between 1021.1 and 1021.5 eV, and is ascribed to ZnO [19]. When detected, the Ga $2p_{3/2}$ core level region shows a single peak at 1116.9–1117.1 eV that corresponds, more likely, to Ga_2O_3. Finally, the Zr $3d_{5/2}$ core level region shows a single peak at 181.6 eV ascribed to ZrO_2 [24]. After *in situ* thermal treatment in H_2 at 573 K for 1 h, the Cu $2p_{3/2}$ core level (Fig. 2B) region of CZZ, $Ga_{0.2}$-CZZ and $Ga_{0.5}$-CZZ exhibits a single peak centred at ~931.8 eV, which can be ascribed to Cu^0 species. However, the samples with higher Ga loadings ($Ga_{1.0}$-CZZ and $Ga_{3.0}$-CZZ) show two Cu $2p_{3/2}$ peaks: a major one at 931.8 ± 0.2, and a minor one at 933.4 eV. The precise assignment of these species is not straightforward from XPS data alone. Although the peak at *ca.* 933.4 eV accounts to Cu^{2+}, the species responsible for the peak at *ca.* 931.8 eV could be either Cu^0 and/or Cu^+ (as Cu_2O), because Cu^0 and Cu^+ species display similar Cu $2p_{3/2}$ levels. Regardless of the precise assignment of the copper species, two facts can be deduced from XPS spectra. On the one hand, the thermal treatment in H_2 causes the reduction of CuO to species containing both Cu^0 and Cu^+ oxidation states. On the other hand, the presence of Ga_2O_3 impedes the complete reduction of CuO, as deduced from the component at 933.4 eV and that accounts for *ca.* 20 at % of total Cu species. Previous reports claimed that Cu species in Cu/ZnO ensembles show a Cu $2p_{3/2}$ peak at 933.4 eV [25]. The position of the Ga $2p_{3/2}$ and Zn $2p_{3/2}$ core level regions remains unchanged after the reduction process. The Zr $3d_{5/2}$ core level is significantly affected by the reduction treatment (Fig. 2C), leading to the appearance of a further minor Zr $3d_{5/2}$ component at *ca.* 183.3 ± 0.2 eV. Although this Zr $3d_{5/2}$ component is small, its proportion increases with the increasing loading of Ga_2O_3 in the samples. Although further work is required for an unequivocal assignment of this Zr species, we suggest that in H_2-reduced samples, the increase in binding energy values points out to a higher ionic character of Zr^{4+} ions upon Ga addition, what probably evidences the presence of hydroxyl groups and the formation of $Zr(OH)_4$ species. It should be remarked here that no peaks ascribed to Na species have been observed in the XPS survey analysis (data not shown).

The relative atomic surface abundance of the different elements in the calcined and the *in situ* reduced samples is shown in Table 2. The nominal atomic Zn/Cu ratio is 0.29; however, as observed from the XPS data (Table 2), the surface atomic Zn/Cu ratios of all calcined samples are significantly higher than the nominal values. The same trend is observed for the Zr/Cu ratio: surface Zr/Cu ratios are higher than the nominal values for all samples (ranging between 0.45 and 0.41). Remarkably, both Zn/Cu and Zr/Cu atomic ratio values decrease with the increasing amount of Ga in the samples, suggesting that Ga addition results in a partial segregation of Cu onto the surface of the samples. The same trend is observed for the reduced catalysts; the surface Zn/Cu and Zr/Cu atomic ratios are higher than the nominal values, although they decrease with the increasing content of Ga in the samples. It is also clear from the set of data reported in Table 2 that the reduction treatment decreases the amount of Cu on the surface of the catalysts. On the other hand, the Ga/Cu surface atomic ratios are in good agreement with the nominal values.

The XPS data are consistent with the XRD results, and suggest that the addition of Ga leads to a higher amount of exposed Cu atoms. Table 1 reports the Cu^0 surface area of the reduced samples as determined by N_2O chemisorption. Noticeably, the fraction of exposed Cu^0 increases with the Ga content. As shown in Table 1, the surface area of Cu^0 in the $Ga_{0.3}$-CZZ sample is increased by a 20% when compared to that of CZZ.

Altogether, the characterization results clearly show that the amount of exposed Cu in the calcined and reduced samples increases upon Ga addition. Furthermore, the surface area of Cu^0 species also increases with the amount of Ga. These effects may have a positive impact on the performance of the catalysts in CO_2 hydrogenation reactions.

3.2. CO_2 hydrogenation to CH_3OH with Ga-promoted CZZ catalysts

Fig. 3 shows the temperature dependence of CO_2 conversion values measured with all catalysts, as well as equilibrium conversion predicted from thermodynamics. CO_2 conversion increases and approaches to equilibrium with increasing temperatures. Only CH_3OH and CO were detected among the carbonaceous reaction products. It is clear that the addition of Ga to the CZZ systems possesses a positive effect in the CO_2/H_2 catalytic performance. Thus, $Ga_{3.0}$-CZZ sample shows the highest CO_2 conversion values within temperature range from 463 to 523 K. At higher temperatures, CO_2 conversion values become offset with temperature; this data suggest that CO2 conversion value will become constant at higher pressures. Not only Ga-promoted catalysts exhibit higher CO_2 conversions, but also the selectivity to CH_3OH is

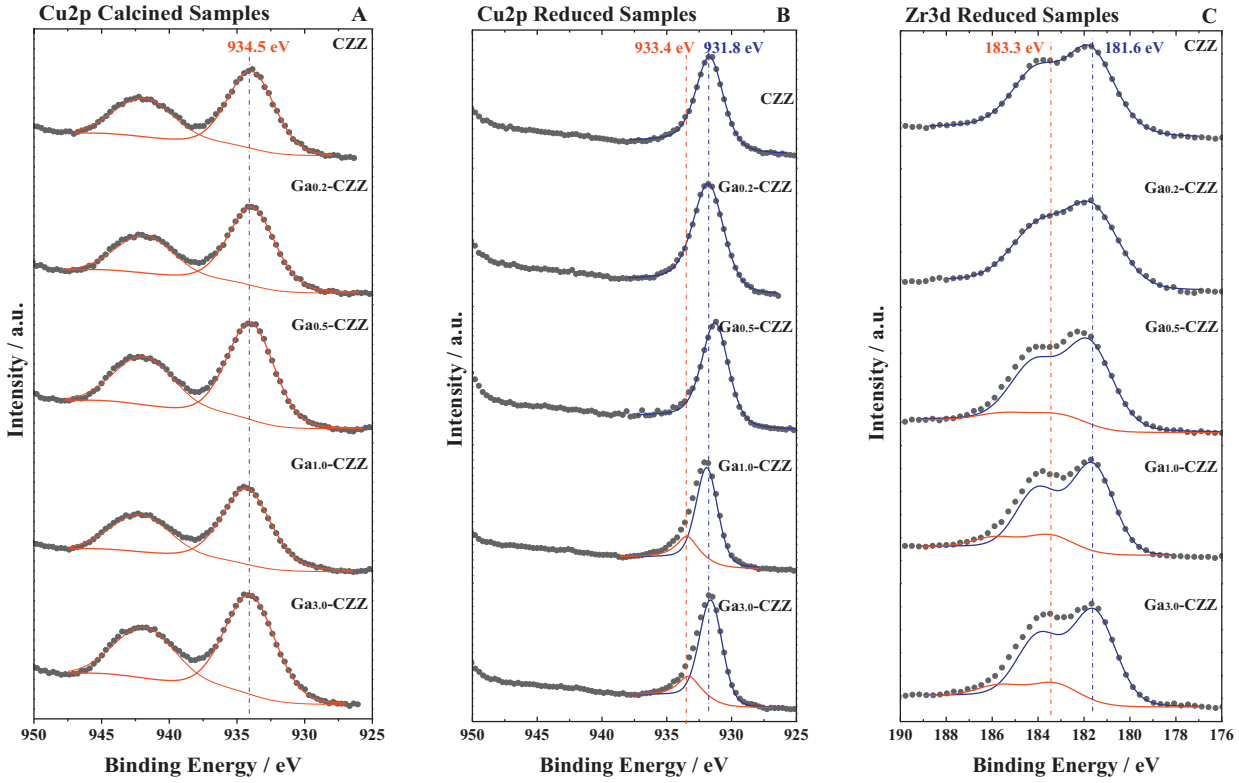

Fig. 2. Cu 2p core level spectra of (a) calcined sample at 673 K, 4 h, ambient air; (b) reduced sample at 573 K, 1 h, H_2 and (c) Zr 3d core level of the reduced sample at 573 K, 1 h, H_2.

superior with the Ga-promoted catalysts. Fig. 4 shows the effect of reaction temperature and catalysts composition on CH_3OH formation rates. Again, the Ga-promoted catalysts present the highest rates for methanol productivity. Thus, the productivity to CH_3OH measured at 463 K with $Ga_{3.0}$-CZZ is *ca.* 30% higher than that obtained with the unpromoted CZZ catalyst. The higher production of methanol with the Ga-promoted catalysts becomes offset by temperature, decreasing to *ca.* 8% at temperatures as high as 523 K. We note here that CH_3OH productivity measured with the $Ga_{3.0}$-CZZ (512 g CH_3OH h^{-1} kg_{cat}^{-1}; 523 K, 3 MPa H_2, 1 MPa CO_2) is amongst the highest reported in literature [26].

In line with the characterization results discussed in the previous section, the high CH_3OH productivity obtained with the Ga-promoted catalysts could be related to the higher amount of Cu on the surface. On one hand, XPS data show that the amount of exposed Cu atoms (as Cu^0 and Cu^+ species) rises when increasing the Ga content in the catalysts. Furthermore, N_2O chemisorption experiments point in the same direction, and reveal that the surface area of metallic Cu increases with the increasing amount of Ga. Previous literature proposed that the activity of Cu-based catalysts for the hydrogenation of either CO or CO_2 was related to: (i) dispersion of Cu species; (ii) presence of Cu^0/Cu^+ pairs, and/or

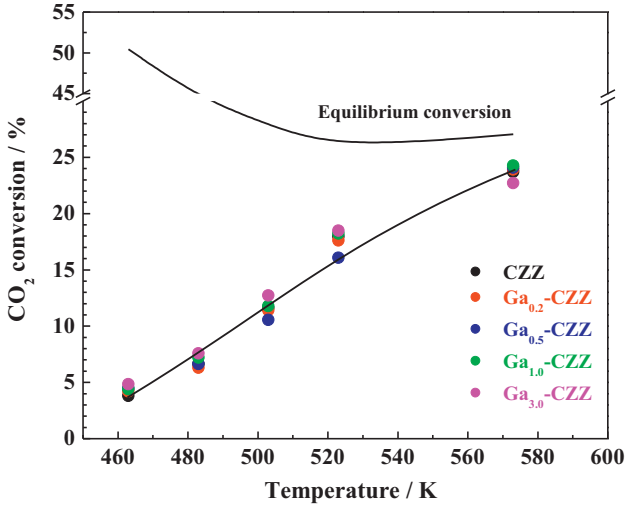

Fig. 3. Effect of reaction temperature on measured CO_2 conversion values. Reaction conditions: 1500 cm^3 h^{-1} g_{cat}^{-1}, 3 MPa H_2, 1 MPa CO_2.

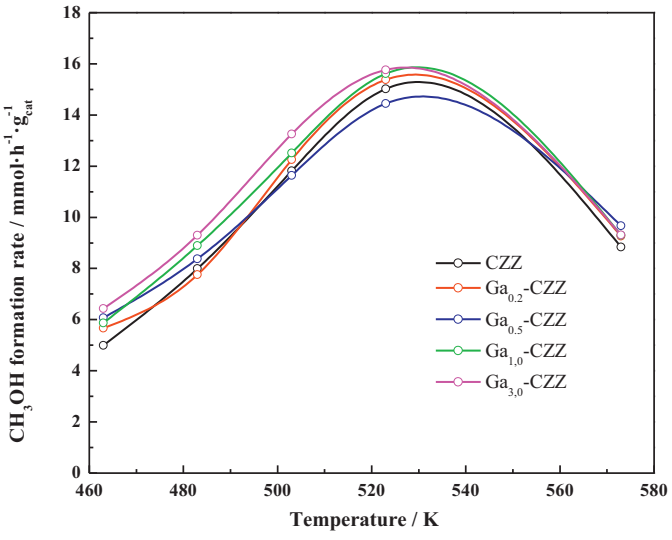

Fig. 4. Effect of reaction temperature on measured methanol formation rates. Reaction conditions: 15,000 cm^3 h^{-1} g_{cat}^{-1}, 3 MPa H_2, 1 MPa CO_2.

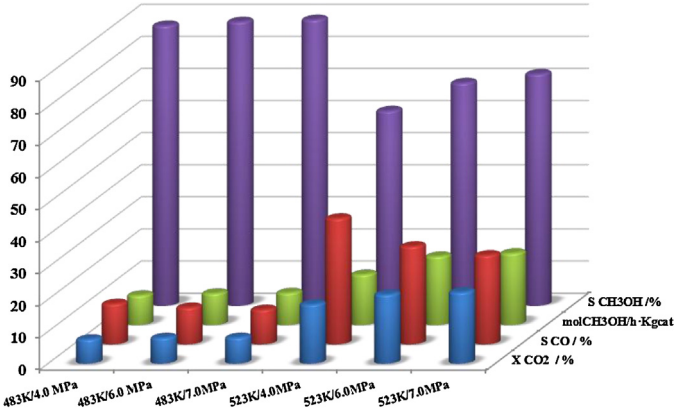

Fig. 5. CO_2 conversion (X_{CO_2}), selectivity to CO (S_{CO}) and methanol (S_{CH_3OH}), and methanol formation rates measured with $Ga_{3.0}$-CZZ catalyst at different temperatures and reactants pressures ($H_2/CO_2 = 3$).

(iii) increased surface area of $Cu/ZnO/ZrO_2$ ensembles [10,27]. Our data clearly show that the productivity of CH_3OH increases with the increasing amount of exposed Cu atoms (as deduced from the higher Cu/Zn and Cu/Zr surface atomic ratios derived from XPS) and with the increasing surface area of Cu^0. These latter species are also responsible for the production of H_2O *via* RWGS reaction. Indeed, a recent theoretical study has shown that CO_2 hydrogenation to CH_3OH on Cu(1 1 1) model surfaces is promoted by H_2O molecules [28].

As expected, the selectivity to CO increases with the increasing the reaction temperature hence decreasing CH_3OH formation. Therefore, in order to obtain high CH_3OH yields, it is preferred to perform the $H_2 + CO_2$ reaction at high pressures rather than at high temperatures. The catalytic performance of $Ga_{3.0}$-CZZ, which shows the lowest yield to CO, has been evaluated for the CH_3OH synthesis from CO_2/H_2 mixtures at 6.0–7.0 MPa at 483–523 K. Fig. 5 and Table 3 compare CO_2 conversions (X_{CO_2}), selectivity to CH_3OH and CO (S_{CH_3OH} and S_{CO}), and CH_3OH synthesis rate (r_{CH_3OH}) obtained with $Ga_{3.0}$-CZZ at the different reaction conditions reported in this manuscript. Fig. 3 shows that the equilibrium conversion of CO_2 decreases with the working temperature. By contrary, CO and CH_3OH formation rates increase with the reaction temperature, especially the former. This is more clearly observed in Figs. 5 and 6. Clearly, the production of CO *via* the reverse water–gas shift reaction becomes significant at higher temperatures and as a consequence the selectivity towards CH_3OH production decreases from values between *ca.* 87 and 89% to values ranging between *ca.* 72 and 61%. It is worth to remark that the selectivity to CO is of at least three fold higher when working at higher temperatures. The effect of the reaction pressure is not dominant when working at 483 K. However, pressure plays a dominant role at 523 K. Fig. 5 shows that both the selectivity towards CH_3OH and the CH_3OH production rate increase with the increasing pressure. On the other hand, the production of CO follows the opposite trend and it decreases with the increasing pressure.

Table 3
CO_2 conversion (X_{CO_2}), selectivity to CO (S_{CO}) and methanol (S_{CH_3OH}), and methanol formation rates (r_{CH_3OH}) measured with $Ga_{3.0}$-CZZ catalyst at different temperatures and reactants pressures ($H_2/CO_2 = 3$).

T (K)	P (MPa)	C_{CO_2} (%)	S_{CO} (%)	S_{CH_3OH} (%)	mol_{CH_3OH} (h kg_{cat})
483	4.0	8	13	87	9
483	6.0	8	11	89	10
483	7.0	8	11	89	10
523	4.0	18	39	61	16
523	6.0	22	31	69	21
523	7.0	22	28	72	22

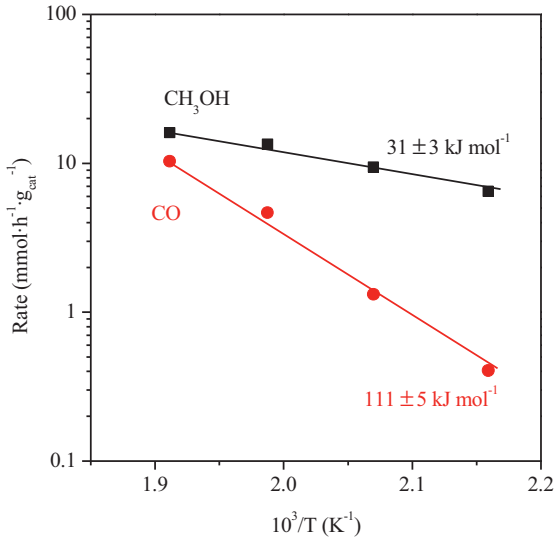

Fig. 6. Arrhenius plots for methanol and CO formation rates measured with $Ga_{3.0}$-CZZ (463–523 K, 2.7 MPa H_2, 1.3 MPa CO_2, 5–19% CO_2 conversion).

3.3. *Kinetic analysis of CO_2/H_2 reaction with $Ga_{3.0}$-CZZ catalyst*

This section is a detailed kinetic analysis of the performance of $Ga_{3.0}$-CZZ for the hydrogenation of CO_2 to methanol. The influence of reaction temperature (463–523 K) on methanol and CO formation rates from H_2/CO_2 mixtures is shown in Fig. 6. These Arrhenius plots reveal a significant influence of reaction temperature on CO formation rates, with a measured activation energy much higher than that for CH_3OH formation (111 ± 5 and 31 ± 3 kJ mol^{-1}, respectively). Our data are consistent with previous works on Cu/ZrO_2 catalysts (473–533 K, 1.29 MPa H_2, 0.43 MPa CO_2) reporting much higher activation energies for CO formation rates (93 and 48 kJ mol^{-1} for CO and methanol formation rates, respectively) [29]. This is the reason as to why our measured rate data clearly show that CO_2 is more selectively hydrogenated to yield CH_3OH when relatively low reaction temperatures are used.

Fig. 7 shows the CH_3OH synthesis rates measured with $Ga_{3.0}$-CZZ catalyst at 523 K as a function of H_2 (0.2–3.0 MPa H_2, 0.4 MPa CO_2) and CO_2 (0.1–1.2 MPa CO_2, 1.0 MPa H_2) pressures (He was used as a balance to maintain constant the total pressure). CH_3OH synthesis rates are proportional to H_2 pressure (first order); in contrast, rates were initially proportional to CO_2 pressures, but the slope of the curve decreases monotonically with the CO_2 pressure in the reactants stream. This trend indicates that methanol formation rate levels off with the CO_2 pressure and suggests that CH_3OH conversion rate will reach a plateau value at higher CO_2 pressures than those reported in this work. Our data are consistent with Le Peltier et al. [18], who suggested that CH_3OH formation from H_2/CO_2 follows an Eley-Rideal type mechanism where adsorbed CO_2 species (CO_2^*) react with molecular H_2 in the slow step of the reaction. Scheme 1 shows a sequence of elementary steps involving CO_2 adsorption and subsequent reaction with molecular H_2 to form the reaction intermediates involved in CH_3OH synthesis:

The quasi-equilibrium assumption for CO_2 adsoprtion and CO_2^* as the most abundant reaction intermediates (MARI) for Scheme 1 gives:

$$r_{CH_3OH} = \frac{K_1 K_2 \cdot P_{CO_2} \cdot P_{H_2}}{1 + K_1 \cdot P_{CO_2}} \quad (4)$$

At low CO_2 pressures ($K_1 \cdot P_{CO_2} \gg 1$), Eq. (4) becomes:

$$r_{CH_3OH} = K_1 K_2 \cdot P_{CO_2} \cdot P_{H_2} \quad (5)$$

which is consistent with our data and previous reports [30].

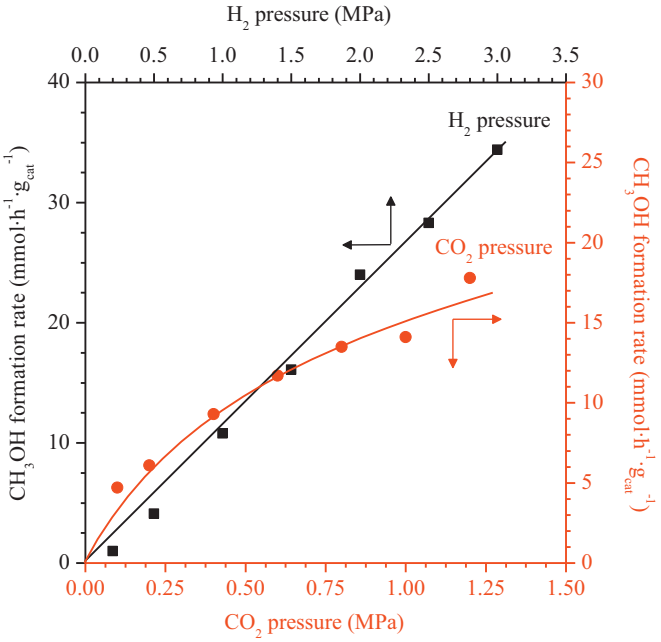

Fig. 7. Influence of H_2 (0.2–3.0 MPa H_2, 0.4 MPa CO_2) and CO_2 (0.1–1.2 MPa CO_2, 1.0 MPa H_2) pressures on methanol synthesis rates measured at 523 K with $Ga_{3.0}$-CZZ.

$$CO_2 + * \leftrightarrow CO_2^* \;:\; K_1$$

$$CO_2^* + H_2 \rightarrow [I^*];\; k_2$$

$$[I^*] + H_2 \rightarrow \cdots \rightarrow \cdots \rightarrow CH_3OH + H_2O$$

Scheme 1. Elementary steps (Eley–Rideal mechanism) in CO_2 hydrogenation to CH_3OH.

Nonetheless, our experimental data (first order in CO_2 and H_2 pressures) would be also consistent with a Langmuir–Hinshelwood type pathway at low CO_2 and H_2 surface coverages (CO_2* and H*, respectively) and assuming quasi-equilibrated CO_2 and H_2 adsorption, and a second hydrogenation step of the intermediate as rate-limiting (Scheme 2).

Indeed, previous studies have suggested that CH_3OH synthesis on Cu-based catalysts proceeds through CO_2 reaction with hydrogen *via* either an Eley–Rideal or Langmuir–Hinshelwood to form formate ($HCOO^*$), dioxomethylene (H_2COO^*), formaldehyde (CH_2O^*), methoxy (CH_3O^*), and finally, methanol (CH_3OH), with all these hydrogenation steps as rate-limiting. The exact identity of the elementary steps involved in CO_2 hydrogenation to CH_3OH still remains unresolved in the literature and is the subject of intensive investigations.

Interestingly, the opposite effects of H_2 and CO_2 pressures on CH_3OH formation rates are found (Fig. 7). These rates increases proportionally at all CO_2 pressures (0.1–1.2 MPa CO_2, 1.0 MPa H_2) and

$$CO_2 + * \leftrightarrow CO_2^*;\; K_1$$

$$H_2 + 2^* \leftrightarrow 2H^*;\; K_2$$

$$CO_2^* + 2H^* \rightarrow \cdots \rightarrow \cdots \rightarrow CH_3OH + H_2O;\; K_3$$

Scheme 2. Elementary steps (Langmuir–Hinshelwood mechanism) in CO_2 hydrogenation to CH_3OH.

at relatively low H_2 pressures (0.0–0.4 MPa H_2, 0.4 MPa CO_2), but they are mostly independent for H_2 pressures > 0.4 MPa. Therefore, selective CH_3OH production at elevated rates requires the use of high H_2 pressures while maintaining CO_2 pressures relatively low.

The observed kinetic effects of temperature (463–523 K) and reactants pressure (0.1–1.2 MPa CO_2, 0.2–3.0 MPa H_2) on methanol formation rates can be described as a power rate law equation:

$$r_{CH_3OH} = k_{0,CH_3OH} \cdot e^{-E_a/RT} \cdot P_{H_2}^{x} \cdot P_{CO_2}^{y} \quad (6)$$

where $E_a = 31\ kJ\ mol^{-1}$, $x = 1.18$, and $y = 0.53$. Similarly, the influence of experimental conditions (463–523 K, 0.1–1.2 MPa CO_2, 0.2–3.0 MPa H_2) on CO synthesis rates are well described as follows:

$$r_{CO} = k_{0,CO} \cdot e^{-E'_a/RT} \cdot P_{H_2}^{n} \cdot P_{CO_2}^{m} \quad (7)$$

where $E_a = 111\ kJ{\cdot}mol^{-1}$, $n = 0.15$; and $m = 0.67$.

4. Conclusions

We show here that CO_2 can be used as a carbon precursor to producing the highly demanded chemical CH_3OH using Cu/ZnO based catalysts. We demonstrate that Ga-promoted Cu/ZnO/ZrO_2 catalysts are highly effective for the selective production of CH_3OH from CO_2 and H_2. The promotional effect can be ascribed to a selective segregation of Cu towards the surface, thus increasing the number of active sites. The effects of reaction temperature and pressure have been also explored. CO_2 conversion increases with the reaction temperature; however, selectivity to CH_3OH decreases at higher temperatures. The kinetic analysis reveals that methanol productivity predominates *versus* CO production at high H_2 pressures.

Acknowledgements

We gratefully acknowledge financial support from the Spanish Ministry of Science and Innovation(MICINN, project ENE2010-15381 and project CENIT-CO2) and the Madrid Regional Government (S2009/ENE-1743). JMGC and RML acknowledge MICINN (*Formación de Profesorado Universitario* programme, FPU) and Madrid Regional Government, respectively, for PhD grants. M. Ojeda is also grateful to the MICINN for a *Ramon y Cajal* contract (RYC-2010-06067).

References

[1] S. Chunshan, Catalysis Today 115 (2006) 2–32.
[2] F.J. Pérez-Alonso, M. Ojeda, T. Herranz, S. Rojas, J.M. González-Carballo, P. Terreros, J.L.G. Fierro, Catalysis Communications 9 (2008) 1945–1948.
[3] T. Herranz, S. Rojas, F.J. Pérez-Alonso, M. Ojeda, P. Terreros, J.L.G. Fierro, Applied Catalysis A – General 311 (2006) 66–75.
[4] R.W. Dorner, D.R. Hardy, F.W. Williams, H.D. Willauer, Energy Environment Science 3 (2010) 884–890.
[5] T. Mokrani, M. Scurrell, Catalysis Reviews – Science and Engineering 51 (2009) 1–145.
[6] C. Ratnasamy, J.P. Wagner, Catalysis Reviews – Science and Engineering 51 (2009) 325–440.
[7] Y. Yang, J. Evans, J.A. Rodriguez, M.G. White, P. Liu, Physical Chemistry Chemical Physics 12 (2010) 9909–9917.
[8] G.C. Chinchen, P.J. Denny, D.G. Parker, M.S. Spencer, D.A. Whan, Applied Catalysis 30 (1987) 333–338.
[9] P.L. Spath, D.C. Dayton, National Renewable Energy Laboratory, 2003 http://www.osti.gov/bridge
[10] D. Grandjean, V. Pelipenko, E.D. Batyrev, J.C. van den Heuvel, A.A. Khassin, T.M. Yurieva, B.M. Weckhuysen, Journal of Physical Chemistry C 115 (2011) 20175–20191.
[11] V.R. Surisetty, A.K. Dalai, J. Kozinski, Applied Catalysis A – General 404 (2011) 1–11.
[12] X. Guo, D. Mao, G. Lu, S. Wang, G. Wu, Journal of Molecular Catalysis A: Chemical 345 (2011) 60–68.
[13] S.E. Collins, D.L. Chiavassa, A.L. Bonivardi, M.A. Baltanás, Catalysis Letters 103 (2005) 83–88.

[14] M. Saito, T. Fujitani, M. Takeuchi, T. Watanabe, Applied Catalysis A – General 138 (1996) 311–318.
[15] T. Fujitani, M. Saito, Y. Kanai, T. Watanabe, J. Nakamura, T. Uchijima, Applied Catalysis A – General 125 (1995) L199–L202.
[16] M. Saito, M. Takeuchi, T. Watanabe, J. Toyir, S. Luo, J. Wu, Energy Conversion and Management 38 (Suppl.) (1997) S403–S408.
[17] J. Toyir, R. Miloua, N.E. Elkadri, M. Nawdali, H. Toufik, F. Miloua, M. Saito, Physics Procedia 2 (2009) 1075–1079.
[18] F. Le Peltier, P. Chaumette, J. Saussey, M.M. Bettahar, J.C. Lavalley, Journal of Molecular Catalysis A: Chemical 132 (1998) 91–100.
[19] J. Toyir, P. Ramírez de la Piscina, J.L.G. Fierro, N. Homs, Applied Catalysis B – Environmental 29 (2001) 207–215.
[20] J. Toyir, P. Ramı̃rez de la Piscina, J.L.G. Fierro, N. Homs, Applied Catalysis B – Environmental 34 (2001) 255–266.
[21] G.C. Chinchen, C.M. Hay, H.D. Vandervell, K.C. Waugh, Journal of Catalysis 103 (1987) 79–86.
[22] G.C. Chinchen, K.C. Waugh, D.A. Whan, Applied Catalysis 25 (1986) 101–107.
[23] J. Słoczyński, R. Grabowski, P. Olszewski, A. Kozłowska, J. Stoch, M. Lachowska, J. Skrzypek, Applied Catalysis A – General 310 (2006) 127–137.
[24] I. Sádaba, M. Ojeda, R. Mariscal, J.L.G. Fierro, M. López Granados, Applied Catalysis B – Environmental 101 (2011) 638–648.
[25] S.V. Didziulis, K.D. Butcher, S.L. Cohen, E.I. Solomon, Journal of the American Chemical Society 111 (1989) 7110–7123.
[26] W. Wang, S. Wang, X. Ma, J. Gong, Chemical Society Reviews 40 (2011) 3703–3727.
[27] F. Arena, G. Italiano, K. Barbera, S. Bordiga, G. Bonura, L. Spadaro, F. Frusteri, Applied Catalysis A – General 350 (2008) 16–23.
[28] Y.F. Zhao, Y. Yang, C. Mims, C.H.F. Peden, J. Li, D. Mei, Journal of Catalysis 281 (2011) 199–211.
[29] R.A. Koeppel, A. Baiker, A. Wokaun, Applied Catalysis A – General 84 (1992) 77–102.
[30] X. An, Y. Zuo, Q. Zhang, J. Wang, Chinese Journal of Catalysis 17 (2009) 88–94.